A phenomenological approach of joint density of states for the determination of band structure in the case of a semi-metal studied by FT-STS

2007 J. Phys.: Condens. Matter 19 355009

(http://iopscience.iop.org/0953-8984/19/35/355009)

IOP PUBLISHING JOURNAL OF PHYSICS: CONDENSED MATTER

J. Phys.: Condens. Matter **19** (2007) 355009 (14pp) doi:10.1088/0953-8984/19/35/355009

A phenomenological approach of joint density of states for the determination of band structure in the case of a semi-metal studied by FT-STS

L Simon[1], **F Vonau and D Aubel**

Laboratoire de Physique et de Spectroscopie Electronique, CNRS-UMR7014, 4, rue des Frères Lumière, 68093 Mulhouse, France

E-mail: l.simon@uha.fr

Received 15 March 2007, in final form 19 April 2007
Published 20 August 2007
Online at stacks.iop.org/JPhysCM/19/355009

Abstract

The authors show that an accurate determination of the band structure can be achieved by using Fourier transform scanning tunnelling microscopy (FT-STM) techniques in the case of a semi-metallic $ErSi_2$ layer grown on a Si(111) substrate. This material provides an ideally confined 2D electron and hole gas that is reflected in a complex standing wave pattern at 77 K. The quasi-particles exist over a wide energy range from −800 to +300 meV without mixing with silicon bulk excitations. The Fourier transform of dI/dV maps have been successfully interpreted using the concept of the joint density of states (JDOS), which will be properly introduced. We present here an intuitive interpretation of the quasiparticle interference process based on a geometric construction which also allows us to clearly demonstrate that hole–hole and hole–electron quantum interferences dominate over electron–electron quantum interference.

(Some figures in this article are in colour only in the electronic version)

An important result in solid-state physics over the last 50 years is the theoretical description of the asymptotic form of the screened potential by a point defect in a uniform electron gas, called Friedel oscillations [1]. These oscillations result from electron–electron interaction and a response to a positive charge held in a quasi-free electron gas in order to reduce the field induced by this singularity. In a linear approximation, the dependence of the induced charge density on the total potential is given in reciprocal space by [2]: $\rho^{\mathrm{ind}}(q) = \chi(q)\phi(q)$.

The susceptibility $\chi(q)$ in the case of the Lindhard theory is given by:

$$\chi(q) = \sum_k \frac{f(k) - f(k+q)}{E_k - E_{k+q}} \tag{1}$$

[1] Author to whom any correspondence should be addressed.

where $f(k)$ is the Fermi–Dirac distribution. This expression simply shows that the main contribution to the charge density variation occurs for $E_{\vec{k}} = E_{\vec{k}+\vec{q}}$, i.e. $\vec{q}$ wavevectors which connect two points of the constant energy contour (CEC) of states. In the case of a nearly-free electron gas ($E(k) = \hbar^2 k^2/2m^*$), all points are connected for the vector $\vec{q}$ with a length $|\vec{q}| = 2|\vec{k}|$, and the energy-resolved charge density oscillates with a wavevector length $\vec{q} = 2\vec{k}$. This asymptotic form of the screening is the basis of the description of the indirect coupling between magnetic moments via the conduction electrons in a metal with the famous Ruderman–Kittel–Kasuya–Yosida (RKKY) interaction potential [3–5] and, for example, the long-range adsorbate interaction mediated by a two-dimentional electron gas [6].

Historically, an important question was: how do these oscillations really reflect the Fermi surface?

Following the work of Friedel, this problem has been considered theoretically in the case of a metal transition by Gautier and Lenglart [7]. However, these oscillations were very difficult to observe, as they were investigated indirectly and in bulk material (three dimensions, 3D). Indeed, in the example of Friedel oscillations created by point-like defects, the amplitude of the oscillations falls off with a distance r as $1/r^{\alpha}$, where α is the dimension of the electron gas that is considered. The development of the scanning tunnelling microscopy and the possibility of imaging the electron density of states in real space has offered the possibility of studying the standing waves, which are in fact *an energy-resolved Friedel oscillation* for two-dimensional (2D) or one-dimensional (1D) electron gas, which provides longer coherence lengths than those observed in 3D. The first standing waves in the local density of surface states (LDOS) was obtained by Hasegawa and Avouris [8] on confined Shockley states of an Au(111) surface at room temperature (RT) and by Crommie *et al* [9] on Cu(111) at 4 K. More recently, the dispersion curve $E(k)$ of surface state electrons of Ag(111) and Cu(111) has been measured, providing at the same time an estimation of the surface state inelastic lifetime [10]. As large energies are accessible both below and above the Fermi level, the deviation of the free-electron-like parabolic dispersion could be also studied. Bürgi *et al* [11] defined a method to image the potential landscape on Au(111) directly by STM. Such measurements have been performed by studying the standing wave generated by a specific step then dealing with a particular reciprocal lattice direction of the Fermi surfaces.

Sprunger *et al* [12] showed the possibility of using STM to image the surface Fermi contour of a metal surface directly by performing the power spectrum of a topographic image of a complex 'electron sea' pattern generated by a random distribution of point-like surface defects. These studies were performed around the Fermi level (low bias voltage) on a simple isotropic Fermi surface of noble metal Au(111) and Cu(111) surfaces [13]. In a nutshell, for this nearly-free electron gas, Friedel oscillations appear in the power spectrum as a circular feature centred around the Brillouin zone centre, with a radius corresponding to $2k_{\mathrm{f}}$. Then this technique was successfully applied to Be($10\bar{1}0$) and Cu(110) systems [14], which have more complex Fermi surfaces compared to previous isotropic Fermi contours. More recently, this technique has been applied to conductance images ($\mathrm{d}I/\mathrm{d}V$ map) related to the LDOS in a short range of energy around the Fermi level in order to characterize high-T_{C} superconductors [15, 16]. Another possibility of this approach has been shown [17]: as two waves with opposite spin directions cannot generate quasi-particle interference (QPI), the authors demonstrated the ability to probe indirectly the orientation of the spin associated with a Fermi surface of a half-magnetic material. These results reveal the importance of this new Fourier transform scanning tunnelling spectroscopy (FT-STS) technique. Here we will apply this approach and test its strength on a semi-metal where some CEC are split into several bands and over wide energy windows in order to determine the whole 2D band structure. We will also show that the power spectrum features can easily be deduced on the basis of the joint density of state (JDOS), which

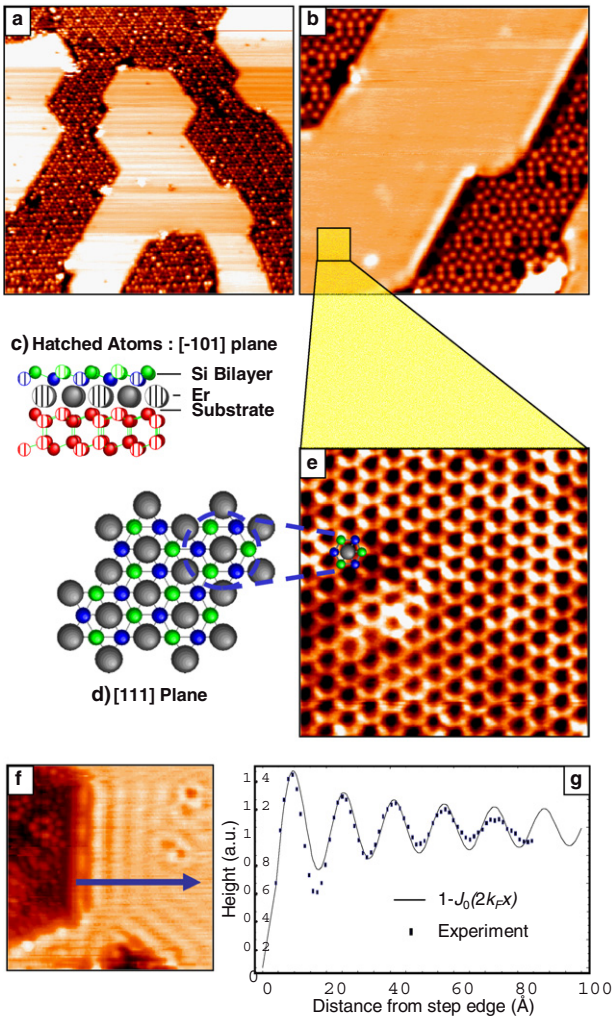

Figure 1. ((a), (b)) Topographic images of $ErSi_2$ islands on Si(111): (a) 50 × 50 nm^2, −1.8 V, 3.1 nA; (b) 19 × 19 nm^2, +1.3 V, 0.5 nA. ((c), (d)) Schematic drawing of the adopted $ErSi_2$ structure projected along the $[\bar{1}01]$ direction: (c) and top view (d) from Stauffer *et al* [20]. (e) Atomic-resolution image in constant-current mode of a $ErSi_2$ plane taken at 77 K (4.5 × 4.5 nm^2, −16 mV, 0.16 nA). (f) Wave pattern close to an $ErSi_2$ step edge (4.5 × 4.5 nm^2, −69 mV, 0.8 nA) and (g) LDOS modulation along the profile taken in (e).

can be evaluated by a simple geometrical construction. This work is an extended version of two previous articles [26, 27] and finally gives an exemplarily phenomenological demonstration of what was previously proposed by Blandin [19] for the generalization of Friedel oscillation in the case of Bloch wave states and by Roth *et al* [18] for the theoretical determination of Kohn anomalies in the study of RKKY interactions for nonspherical Fermi surfaces. Discrepancies between our proposed construction and Roth's approach is outside the scope of this paper and will be discussed elsewhere.

The system investigated here is erbium disilicide grown on Si(111) 7 × 7. This has been studied extensively by photoemission and theoretical calculations [20, 21], and an atomic model of this structure has been determined by the team of Gewinner [20, 23]. Figures 1(c), (d) show

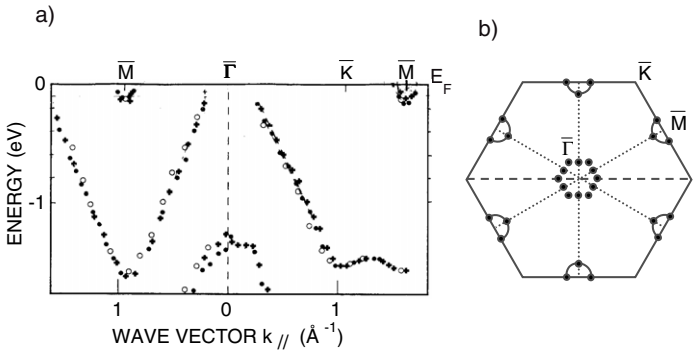

Figure 2. (a) Experimental band structure obtained by ARPES: He_I(●), He_{II}(○) and Ne_I(+). (b) Deduced Fermi surface from Wetzel *et al* [21].

a schematic drawing of the adopted structure, which has subsequently been amply confirmed by several groups [24, 25]. This structural model consists of a p(1 × 1) plane of erbium atoms inserted between the silicon substrate and a buckled silicon layer (see figure 1(c)). Figure 2 shows the Fermi surface and the band structure determined by conventional angle-resolved phoemission spectroscopy (ARPES) from Wetzel *et al* [21]. This system leads to a perfect 2D metal–semiconductor interface which shows a semi-metallic character with a hole pocket centred around the centre of the surface Brillouin zone $\overline{\Gamma}$ and six electron pockets around the $\overline{M}$ symmetry points at the Fermi level (see figure 2(b)). At this stage the exact shape of the electron pocket as well as the dispersion of the hole band near the Fermi level was unknown. Extended Hückel theory calculations [20] showed that the electron pockets around the $\overline{M}$ points of the Brillouin zone are due to a hybridation between the Er_{5d} and Si_{3p} orbitals of the silicon bilayer on top and underneath the erbium plane. Near the $\overline{\Gamma}$ point the Si_{3p_z} feature becomes dominant and localized in the first silicon plane. The hybridation of Er_{5d} with the volume states is extremely weak for binding energies up to 1.3 eV. Thus $ErSi_2$ is a two-dimensional electron gas confined in a 5 Å thick layer. In contrast to the case of Shockley states of metals, where the study is limited to an energy region close to the Fermi level, this system allows a dispersion measurement based on Friedel oscillations with a large energy scale. Moreover, the band structure of erbium silicide is similar to those observed for other rare-earth silicides such as $GdSi_2$ and YSi_2 [33]. This confined 2D electron gas is a highly interesting system for investigating what kind of information the Fourier transform (FT) STM technique provides on the topology and physics of complex Fermi contours. Indeed in this case, compared to an isotropic Fermi contour, the Fermi surface is split into two types of bands and the whole band structure can be studied over a large energy range without any coupling with the substrate band structure.

The experiments were performed with a commercial low-temperature scanning tunnelling microscope (LT-STM) purchased from Omicron. All measurements were taken at 77 K, and in this system both the tip and the sample are at the same temperature. We use a tungsten tip cleaned under ultrahigh-vacuum conditions by resistive heating. The tip is then prepared on a Au(111) surface until we obtain a good atomic resolution at room temperature and a good Fermi level by spectroscopy measurements. A bias voltage V is applied to the sample. Conductance (dI/dV mapping) measurements are performed with a lock-in amplifier using typically $V_{pp} = 50$ mV modulation at 1 kHz on a sample bias voltage without opening the

feedback loop[2]. The deposition of Er is performed at room temperature in the sub-monolayer range, followed by annealing at 800 K.

Figures 1(a) and (b) show typical large-scale images of the resulting surface. We obtain large 2D $ErSi_2$ islands surrounded by 7×7 silicon regions, in agreement with [22, 28]. In accordance with the structural model (figure 1(d)), atomic resolution of the $ErSi_2$ planes shows a p(1 × 1) translation symmetry. The p(1 × 1) arrangement is attributed to the $3p_z$ orbitals of the upper silicon atoms of the 2D $ErSi_2$ surface. However, as shown in figure 1(e), a constant-current image taken at low bias voltage (here −10 mV) reveals that each large bright spot of the previously observed p(1 × 1) splits into two spots of different brightness, which form a hexagon surrounding a black hole. Such a resolution depends critically on the extremely good quality of the tip. Both strong and light spots forming a honeycomb network are unambiguously attributed to the two inequivalent silicon atoms of the buckled layer, as for the up and down Si atoms of the top-most Si bilayer in figure 1(c). Changes in bias polarity (i.e. probing empty states) do not modify the STM image. We deduce that little electron transfer is observed between the silicon atoms of the buckled layer. The dark centre of the hexagon in both bias polarities means that the tunnelling probability between the tip state and Er electron states is negligible, making these atoms difficult to observe.

Figure 1(f) shows a constant-current image of a $ErSi_2$ island surrounded by silicon regions. Standing waves are observed near the surface defects. Ripples parallel to the silicide edges, as indicated on the figure, are clearly visible. Figure 1(g) shows the line profile taken perpendicularly to a step edge. The amplitude of the oscillation is up to 0.20 Å. This experimental profile line is easily fitted by a Bessel function, and the oscillations fall off following roughly a decreasing law as $1/\sqrt{r}$, as expected by the reflection of a nearly-free electron wave at a step edge and routinely observed on noble metals for Shockley states. The measured lengthscale leads to a wavevector $q = 0.40 \pm 0.01$ Å^{-1}. If one assumes that the hole pocket is mainly responsible for the observed ripple, the resulting Fermi wavevector of the standing waves corresponds to $k_f = q/2 = 0.2 \pm 0.02$ Å^{-1}. Angle-resolved photoemission spectroscopy (ARPES) measurements performed at room temperature (see figure 2) show that the nearly filled band crosses the Fermi level at $k_f = 0.15$ Å^{-1} along $\overline{\Gamma M}$ and $k_f = 0.17$ Å^{-1} along $\overline{\Gamma K}$ with an uncertainty of 0.05 Å^{-1} [21].

At the Fermi level, both hole-like and electron-like quasi-particles are able to contribute to the observed standing waves. At this stage, one cannot definitely tell which electron states (holes or electrons) actually contribute to the observed ripples parallel to a silicide edge. We will see that the FT-STM technique is able to solve this question. Figure 3(a) shows a typical complex standing-wave pattern obtained near the Fermi level with a superimposed well-defined atomic resolution. The corresponding power spectrum is represented in figure 3(b) and looks similar whatever the scanned region is, but some features are more or less intense. It shows a circle with a radius $q = 0.42 \pm 0.04$ Å^{-1}. The reciprocal lattice spots provide a direct calibration of the FT image. Six spots where the intensity is enhanced and lying on the contour are clearly visible. These are positioned along the $\overline{\Gamma M}$ directions. In the same direction, six features are located around the $\overline{M}$ points, i.e. for $q = 0.945$ Å^{-1}.

We now want to address the origin of the observed FT pattern. This system shows some similarities with that studied by Petersen *et al* [13], i.e. a Cu(110) surface, a surface orientation

[2] A possible convolution of the LDOS with a tip–sample distance variation has to be taken into account (see [32] and references therein). This was minimized by considering the topographic image instead of dI/dV map for an energy below 100 meV. As such, a convolution especially disturbs the phase shift of the scattering; performing a fast Fourier transform (FFT) power spectrum avoids this problem.

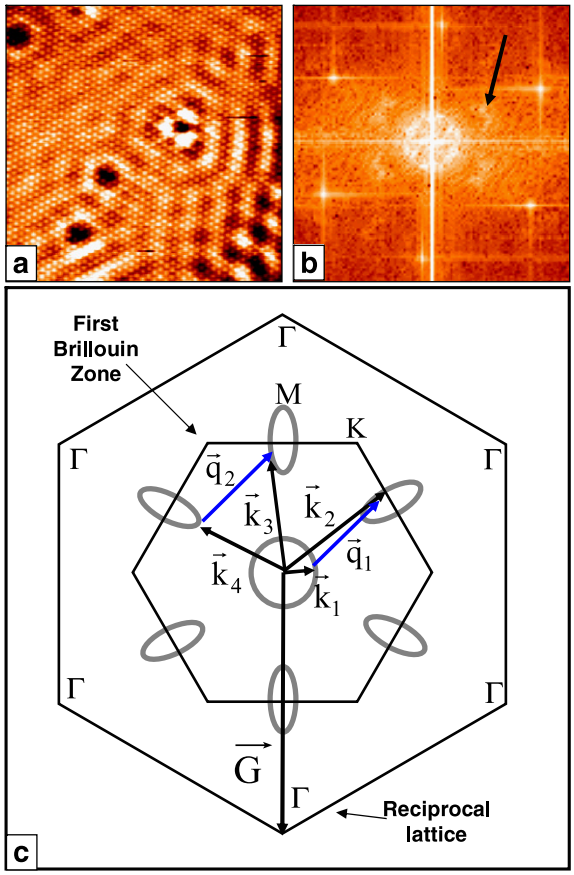

Figure 3. Constant-current images: (a) 16 × 16 nm, −17 mV, $I = 2.37$ nA, taken at 77 K; (b) corresponding power spectrum of the Fourier transform; (c) expected surface Fermi contour and wavevectors $\vec{q} = \vec{k}_i - \vec{k}_j$ that might contribute to the standing-wave pattern.

which exhibits two electron pockets and leads to a shifted Fermi contour image in the FT image from the higher-order diffraction spots to the centre of the first Brillouin zone.

Here the erbium disilicide is semi-metallic and the Fermi contour is discontinuous. Theoretically, in a general point of view of perturbation theory, possible $\vec{q}$ vectors of the standing-wave pattern can be generated by $\vec{q} = \vec{k} - \vec{k}' + \vec{G}$, where $\vec{k}$ and $\vec{k}'$ correspond to Bloch states of the isoenergetic contour and $\vec{G}$ is a reciprocal lattice vector [16]. In our case, standing wavevectors can be inferred from figure 3(c), where $\vec{k}_1$ describes the contour of the central hole pocket and different wavevectors $\vec{k}_i, i > 1$, point the electron pockets around $\overline{\mathrm{M}}$. Within our uncertainty and that of the published photoemission data, we attribute the central circle of the power spectrum rather to the hole pocket which essentially reflects scattering of hole states $\vec{k}_1$ to holes states $-\vec{k}_1$ by defects.

Let us now discuss the features indicated by an arrow in the FT image in figure 3(b) which are located at 0.945 Å^{-1}, i.e. in close proximity to the $\overline{\mathrm{M}}$ points. Among the different combinations of wavevectors in figure 3(c), two possible interpretations of these features have to be considered: either the wavevector corresponding to electron scattering from state $\vec{k}_i$ in

pocket i to $\vec{k_{i+1}}$ in pocket $i+1$ ($\vec{q_2}$) or the combination of wavevectors pointing the hole pocket with an electron pocket ($\vec{q_1}$). Both are able to give scattering events around the $\overline{\mathrm{M}}$ points.

We are then led to consider a quasi-particle interference approach and take into account all possible wavevectors and scattering processes from a wavevector $\vec{k}$ into $\vec{k'}$ of the same isoenergetic contour. If we consider that all these scattering events are equally probable, the weight of a given process is related to *the number of possible wavevectors $\vec{q}$ found with the same length and direction joining two points of the iso-energetic contour of states*. This is in fact a concept of joint density of states (JDOS) for a given iso-energetic contour, which is a quasi-particle scattering interference approximation. To our knowledge, this was first introduced in the high-T_C community following the work of Hoffmann *et al* [15] and McElroy *et al* [16], who evidenced LDOS modulations, observed for energies lower than ∼30 meV. These modulations change with bias voltage and are interpreted as a quasi-particle interferences process. A theoretical basis for the interpretation of their results based on a Green function formalism was proposed by Wang and Lee [29]. More recently, again in the high-T_C superconductor community with $Bi_2Sr_2CaCu_2O_{8+\delta}$ (Bi2212), the relationship between ARPES measurement and the quasi-particle scattering interpretation of FT-STS measurement has been made using the concept of JDOS [30, 31]. The link between the two measurement methods is finally the *real-space single-particle spectra*, which is, in the case of STM, the local density of states and the *momentum-space single-particle spectral function* for ARPES measurements [31].

Here, we will now show the FT-STS measurements in a large energy range and propose a clear interpretation of all observed features by means of the phenomenological approach of the joint density of states (JDOS). Let us introduce properly the concept of JDOS in this particular case of quasi-particle interference. From a theoretical point of view, in the absence of defects the eigenstates of the film are 2D Bloch states, $\psi_{\vec{k}}(\vec{r})$, and the energy-resolved LDOS:

$$n(\vec{r}_0) = \sum_{\vec{k}} |\psi_k(\vec{r}_0)|^2 \delta(E(k) - \omega) \tag{2}$$

can only exhibit Fourier components at reciprocal lattice vectors $\vec{G}$. We consider a 2D Bloch state as:

$$|\vec{k}\rangle = \sum_{\vec{G}} \alpha(\vec{k}, \vec{G}) \mathrm{e}^{\mathrm{i}(\vec{k}-\vec{G})\cdot\vec{r}}. \tag{3}$$

In the presence of defects, a particle in Bloch state $\vec{k}$ can be scattered into a Bloch state $\vec{k'}$ and the new eigenstates can be constructed to the leading order in perturbation theory as linear combinations of the degenerate unperturbed states $\vec{k}$ that belong to the constant energy contour (CEC) $E(k) = \omega$. The linear combination of unperturbed degenerated states is:

$$|\psi\rangle = \sum_{\vec{k}\in S_E} \beta(\vec{k}) |\vec{k}\rangle \tag{4}$$

then,

$$|\psi\rangle = \sum_{\vec{k}\in S_E} \sum_{\vec{G}} \alpha(\vec{k}, \vec{G}) \beta(\vec{k}) \mathrm{e}^{\mathrm{i}(\vec{k}+\vec{G})\cdot\vec{r}}. \tag{5}$$

S_E is the surface of constant energy contour. If the electrons are nearly free, then $\alpha(\vec{k}, \vec{G})$ falls off rapidly for large $\vec{G}$ and the plane waves become dominant. However, $\beta(\vec{k})$ are in form of $o(\delta V)$, where $\delta V(\vec{r})$ is the perturbation of the Hamiltonian by the defects. The charge density for the new eigenstates is:

$$\langle\psi|\psi\rangle = \sum_{\vec{k},\vec{k'},\vec{G}} \alpha(\vec{k}, \vec{G}) \alpha^*(\vec{k'}, \vec{G'}) \beta(\vec{k}) \beta^*(\vec{k'}) \mathrm{e}^{\mathrm{i}(\vec{k'}-\vec{k}+\vec{G})\cdot\vec{r}}. \tag{6}$$

As the energy-resolved density of states is:

$$n(E,\vec{r}) = \frac{1}{4\pi^3}\int_{\vec{q}} \left|\psi_{\vec{q}}(\vec{r})\right|^2 \delta(E - E(\vec{q}))\,\mathrm{d}\vec{q} \tag{7}$$

it becomes:

$$n(E,\vec{r}) = \frac{1}{2\pi}\int \Big[\frac{1}{4\pi^2}\sum_{\vec{k},\vec{k}',\vec{G}} \alpha(\vec{k},\vec{G})\alpha^*(\vec{k}',\vec{G})\beta(\vec{k})\beta(\vec{k}') \times \delta(\vec{q} - (\vec{k}' - \vec{k} + \vec{G}))\delta(E - E(\vec{q}))\Big]\mathrm{e}^{\mathrm{i}\vec{q}\cdot\vec{r}}\,\mathrm{d}\vec{q} \tag{8}$$

which can be written as:

$$n(E,\vec{r}) = \frac{1}{2\pi}\int_{\vec{q}} g(E,\vec{q})\mathrm{e}^{\mathrm{i}\vec{q}\cdot\vec{r}}\,\mathrm{d}\vec{q}. \tag{9}$$

In equation (8), the term between the brackets is a Fourier component of the LDOS at wavevectors $\vec{q} = \vec{k}' - \vec{k} + \vec{G}$ with an amplitude which takes the general form

$$g(\omega,\vec{q}) = \frac{1}{4\pi^2}\int\int_{E(k)=E(k')=\omega} f(\vec{k},\vec{k}',\vec{G})\delta(\vec{q} - \vec{k} + \vec{k}' \pm \vec{G})\,\mathrm{d}^2\vec{k}\,\mathrm{d}^2\vec{k}' \tag{10}$$

where $f(\vec{k},\vec{k}',\vec{G})$ is a weight factor that depends on matrix elements and thus on the overall distribution and nature of defects. $g(\omega,\vec{q})$ is a JDOS with a main contribution for $\vec{G} = 0$ and replicas shifted by $\vec{G}$ for $\vec{G} \neq 0$. $g(\omega,\vec{q})$ may be calculated by solving the Schrödinger equation for simple defect geometries. Yet, if many defects of various symmetries are present, one may assume that $f(\vec{k},\vec{k}',\vec{G})$ is a fairly smooth slowly varying function of $\vec{k}$ and $\vec{k}'$. As can be seen in figure 3(c) for ω at the Fermi energy and the small extent of the hole and electron pockets in reciprocal space, this leads to the approximation adopted here: in the calculation of $g(\omega,\vec{q})$, $f(\vec{k},\vec{k}',\vec{G})$ is taken as a simple (but different) constant for hole–hole, electron–electron and hole–electron contributions, respectively. Finally, we consider the power spectrum of the conductance images. Then, with this approximation and considering the Wiener–Kinchine theorem, which shows that the Fourier transform of the spectral density is the auto-correlation function, we can easily demonstrate that the calculated JDOS picture is the auto-correlation function of the energy-resolved charge density of state diagram.

In practice, JDOS calculation consists of counting the number of $\vec{q}$ wavevectors with the same length and direction corresponding to a scattering event. This corresponds to the reconstruction illustrated figure 4. Here we consider the mixing for two CECs, taking a fixed circular contour and an elliptical contour in which the ratio a/b of the large and small half-axes of the ellipse is varied. The resulting JDOS calculation, displayed in figures 4(c) and (d), changes drastically. This demonstrates the potential accuracy of this approach, based only on geometric construction which, with trained eyes, also allows an intuitive determination of CEC from the power spectrum features, as we will see later.

Let us now come back to the experiment. Figure 5 shows the band structure of $ErSi_2$. In this system, no bulk band state perturbs the perfectly confined 2D electron gas in a large energy range roughly from -1 to 1 V around the Fermi energy and essentially the whole surface Brillouin zone. Three energy regions can be identified in figure 5: in zone I ($E < -200$ meV), only hole band states exist. In zone II (-200 meV $< E < +250$ meV) both hole and electron quasi-particles have to be considered in the QPI process. Zone III ($E > +250$ meV) is the region where only electron band states are involved. This latter region will be discussed elsewhere. In order to probe the whole band structure (see figure 5) we have performed the power spectrum of an STM image with a 25×25 nm^2 scan area with atomic resolution near the Fermi level but also on a $\mathrm{d}I/\mathrm{d}V$ map (conductance image) for different bias voltages.

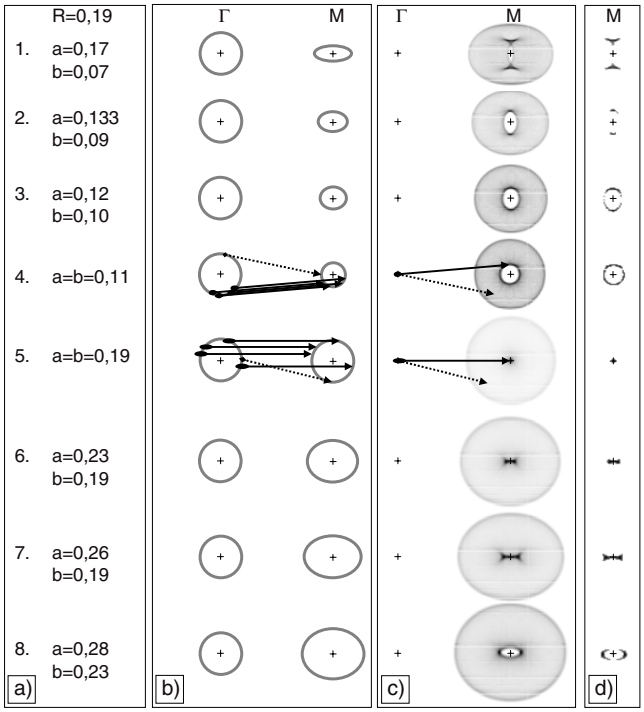

Figure 4. Table illustrating the evolution of the JDOS as a function of the geometric isoenergetic contours. (a) Size of the structures: R, radius of the circle centred at the Γ point; a, b are, respectively, the radii of the large and small half-axes of the ellipse centred at the M point. (b) Representation of the constant energy contour this representation is scaled. (c) Representation of the resulting JDOS in greyscale (the region of high JDOS are black). (d) A greyscale cut-off has been applied to represent the features that are possible to observe in the experimental power spectrum.

Tunneling conditions, the acquisition time and the lock-in time constant have been chosen in order to achieve acceptable signal-to-noise ratio and a $\mathrm{d}I/\mathrm{d}V$ map with atomic resolution on such large-scale images in order to ensure that features with large wavevectors can indeed be observed. With these conditions, replicas of features up to the third Brillouin zone with lower bias voltages remain visible. Power spectra in the first energy windows are displayed in figures 6(a)–(d). The energy is varied from −825 to −226 meV and a hexagon is observed around the first Brillouin zone centre. Its size decreases as the energy increases: this inverse dispersive curve has to be associated with hole–hole QPI. Basically, JDOS calculations for hexagonal constant energy contours with $k = q/2$ in figures 6(e)–(h) confirm the observed feature. The amplitude of the calculated JDOS is represented by a grey scale where an exponential scale intensity was applied to allow a direct comparison with the FFT power spectra. The clear-cut characteristic hexagonal shape nicely reveals the anisotropy of the quasi-particle dispersion in the film plane (see figure 5). We also observe an enhancement of the intensity of the contour in the directions $\overline{\Gamma\mathrm{M}}$ (indicated in figure 6(a)). This is basically a remarkable JDOS effect that strongly favours the $\overline{\Gamma\mathrm{M}}$ directions for a hexagonal contour, as opposed to a simple circular one because of nesting. In this simple isotropic CEC, the evaluation of the JDOS could easily be understood using the schematic geometric construction, as depicted figure 7. Let us compare an hexagonal-shaped CEC and a circular-shaped CEC.

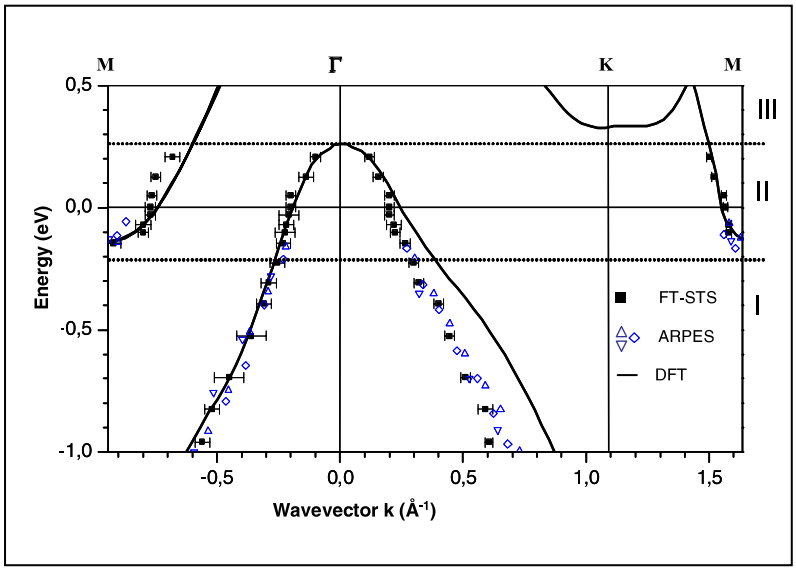

Figure 5. Dispersion curve $E(k)$ of $ErSi_2$ with our FT-STS experimental points (filled squares). The continuous line is the density functional theory (DFT) calculation performed in the case of a similar system, YSi_2 [33]. Empty symbols are RT ARPES measurements [21].

The thickness of the contour illustrates the energy uncertainty given by bias modulation in the conductance image technique. This also represents the wavevector gradient due to the energy range of the mixed unperturbed eigenstates. The JDOS calculation consists of counting the number of $\vec{q}$ wavevectors with the same length and direction corresponding to a scattering events. This is in fact proportional to the intersection area resulting from the translation of the CEC in both directions and the length of the scattering process that is considered. For a circular contour, whatever the direction, this area is the same. An isotropic JDOS contour is then expected, as shown [13]. For an hexagonal contour the scattering process with wavevector $\vec{q}_1$ (direction $\overline{\Gamma K}$) corresponds to an intersection area S_1 that is smaller than S_2 corresponding to the scattering process in the direction $\overline{\Gamma M}$. An anisotropic JDOS hexagonal contour is then expected, as observed experimentally in figure 6. The hole band dispersion in region I deduced from a series of FT-STS measurements[3] is reported in figure 5 for the symmetry directions $\overline{\Gamma M}$ and $\overline{\Gamma K}$, respectively.

Region II: mixed states from hole- and electron-like bands are possible.

Figure 8 shows a series of selected FT-STS measurements in the energy range of region II (see figure 5) crossing the Fermi level where hole–hole, electron–electron and hole–electron QPI are now expected. At −102 meV (figure 8(a)) the FT shows the central hole contour which becomes more circular. Moreover, new features are now observed around the $\overline{M}$ points of the Brillouin zone. While the central hole pocket size reduces with increasing bias voltage, replicas obtained by a translation of the reciprocal lattice vector $\vec{G}$ and electron–electron QPI now complicate the central FT-STS feature. In order to measure the hole dispersion with higher precision, the central hole contour has been taken in the replicas around the centre of higher-order Brillouin zones. Deduced experimental points concerning the dispersion of the hole pocket are plotted in figure 5. The hole band shows an inflexion around −300 meV which

[3] STM movies with FT-STS measurements can be found in the on-line article's HTML reference section.

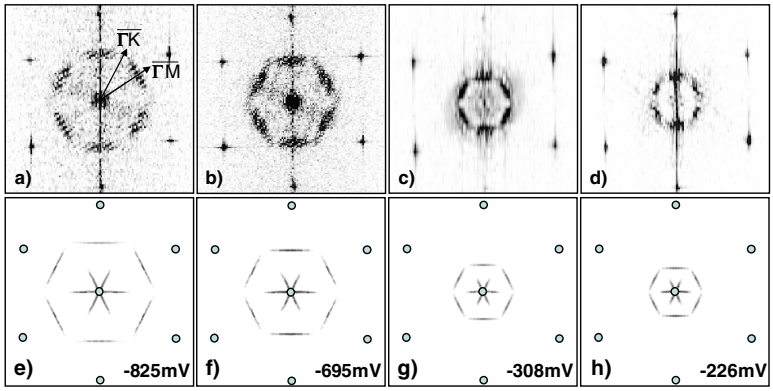

Figure 6. (a)–(d) FT-STS obtained for the energy range from −825 to −226 meV corresponding to region I of figure 5. (e)–(h) Corresponding JDOS calculations for hexagonal CEC.

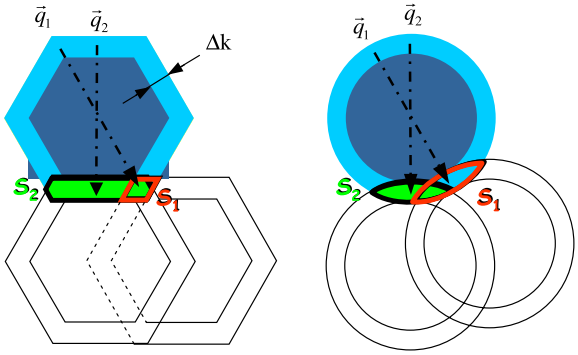

Figure 7. Geometric construction which nicely illustrates the JDOS concept and the nesting effect, which leads to an isotropic or anisotropic JDOS contour in the case of a circular and an hexagonal CEC, respectively.

reduces the anisotropy of the isoenergetic contour in order to obtain a rather more circular contour.

Let us now focus on the intriguing features around the $\overline{\text{M}}$ points which are observed from −146 to +208 meV in figure 8. Changing the energy does not modify their position but only their shape. Indeed, starting from a diffuse structure elongated in the direction perpendicular to $\overline{\Gamma\text{M}}$ at −102 meV, a marked bone-shaped structure is developed near the Fermi level (indicated by an arrow in figure 8(b)). The splitting between spots is reduced for an energy of +49 meV (figure 8(b)), leading to one point at +126 meV (figure 8(d)). Two split spots in the $\overline{\Gamma\text{M}}$ direction are then observed at +208 meV (figure 8(e)). This feature disappears for higher energy and a more complicated FT-STS pattern (not discussed here) is observed. This most remarkable bone-shaped structure observed near the Fermi level can be interpreted in a very transparent and convincing way by JDOS calculations. Indeed, in this energy region (labelled II in figure 5) both electron–electron and hole–electron scattering events can be involved in this feature. As can been see in figure 3(c) around the $\overline{\text{M}}$ point of the Brillouin zone, the vectors $\vec{q}$ are very close to scattering vectors between consecutive electron pockets. This event could also correspond to scattering between hole and electron pockets. These two possibilities

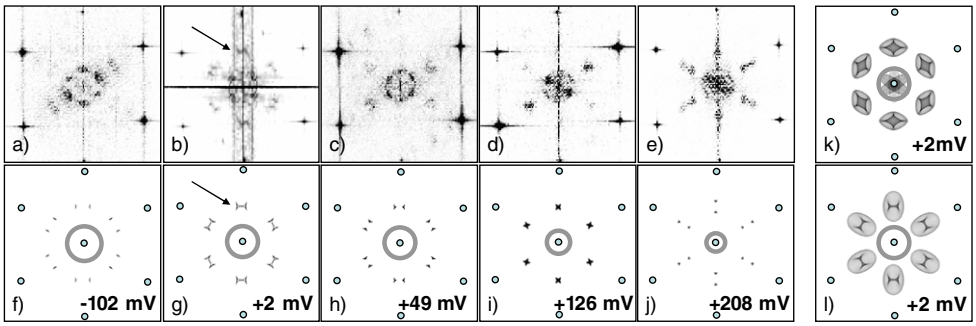

Figure 8. (a)–(e), (f)–(j) Selected FT-STS measurements and joint density of states calculations for energies from −102 to +208 meV corresponding to the region of the band structure labelled II in figure 5. An example of the calculated JDOS for the Fermi level is shown for electron–electron (k) and electron–hole (l) QPI, respectively.

have been tested theoretically by calculating the relevant contributions to the JDOS $g(\omega, \vec{q})$. Figures 8(k) and (l) compare the calculated JDOS for electron–electron and hole–electron events, respectively considering a Fermi surface similar to the one presented in figure 3(c) with a central hole pocket and six ellipses around the $\overline{\mathrm{M}}$ points. For both cases, a complex feature around the $\overline{\mathrm{M}}$ point is observed. If we consider the JDOS for the two events separately, we see that both JDOSs indeed give rise to features around the $\overline{\mathrm{M}}$ point, but the shapes are quite different. For electron–electron scattering the calculations show six features with a definite diamond shape, whereas a clear-cut bone-shaped feature is indeed observed for the hole–electron events. As we observe clearly, for the last one we can readily conclude that this feature in the FT-STS patterns is mainly due to QPI between holes and electrons. Obviously, a weighting factor $f(\vec{k}, \vec{k}', \vec{G})$ that is fairly large for hole–electron events compared to electron–electron events (because of the matrix elements that are involved) could be invoked. We find a remarkably strong sensitivity of the calculated feature geometry in shape and size to the input constant energy contour. The evolution of the shape observed from figures 8(a)–(e), as described before, can be explained nicely by the change in relative size between the small and large ellipse axes a and b, respectively, of the electron pocket and the central hole pocket radius r. The particular bone-shaped feature is observed as long as $r > a$ and the size of the bone depends on the elongation of the ellipse. When $r = a$, one point is observed (see figures 8(d), (i)), and when $r < a$, the features split into two points in the $\overline{\Gamma\mathrm{M}}$ direction, as is indeed observed in figure 8(e). The experimental electron quasi-particle dispersion plotted in figure 5 was obtained by searching for the reconstruction which allows the best fit between the observed FT-STS patterns and the JDOS calculation. The best JDOS fits are depicted in figures 8(f)–(j). The shape evolution of the features near the M points clearly reproduces the observed evolution in the FT-STS patterns. The sensitivity of this approach is so high that it allows us to determine quite accurately the dispersion at the bottom of the electron band and at the top of the hole band. We actually find a very good agreement between the observed features' shape and size at the Fermi level, as for the conservation of charge between holes and electrons, namely, to a very good approximation, that $r^2 = 3a \times b$. Moreover, we obtain the optimal ratio $b/a = 3$ for the electron pocket.

Let us now discuss the experimental FT-STS 2D band structure arrived at in figure 5. In region I, the anisotropies of the hole band structure in directions $\overline{\Gamma\mathrm{M}}$ and $\overline{\Gamma\mathrm{K}}$, respectively, are clearly evidenced by the very typical shape of the central hole feature of FT-STS represented in figure 8. An excellent agreement between our experimental points and previous ARPES

measurements [21] is found. The agreement is also excellent with the calculated band structure from Rogero *et al* [33] in direction $\overline{\Gamma M}$ but not in direction $\overline{\Gamma K}$. Obviously, the YSi_2 DFT-LDA (local density approximation) calculation reproduces the global shape of the measured hole band, but higher-energy excitations are shifted by values as large as 250 meV. For the empty states, a good agreement is recovered. Similar shifts for the predicted surface state energy positions around the K point have been mentioned before for YSi_2 and $GdSi_2$, and the necessity to improve the LDA self-energy term has been noted [33]. In conclusion, we note several important issues. First, fairly simple JDOS calculations and their comparison with FT-STS maps by a trial-and-error method provide a quite accurate determination of the size and shape of even noncircular or free electron-like constant energy contours. This, in turn, provides precise quasi-particle dispersion and fine details of fairly complex 2D band structures. Second, the agreement with angle-resolved photoemission data is excellent, and this indicates that both methods indeed probe the same quasi-particle excitations of the system. Third, defect-induced hole–electron, hole–hole and electron–electron QPI can be evidenced clearly and distinguished and their relative importance assessed experimentally. We have shown here that the power spectrum of a quasi-particle interference pattern of a conductance image is in fact the self-correlation function of the energy-resolved constant energy contour in reciprocal space (JDOS). The success of this method and its ability to measure a complete band dispersion and disentangle the quasi-particle interference effect in our case allows us to discern the weight of the scattering events between hole–hole, hole–electron or electron–electron (-like) quasi-particle remains surprising. As large signal-to-noise ratio is expected, this ability has been discussed by Capriotti *et al* [34] and Kodra and Atkinson [35] in the case of high-T_C superconducting material [15, 16].

In a few words, as first-order stationary perturbation theory is invoked in the background of the Lindhard approach, the crucial point is to deal with a physical system in which the scattering processes mix the unperturbed wavefunctions sufficiently in k-space and also in energy. This signifies that the weight of the matrix elements in the transition process depending on the energy level and the physical process for the type of measurements (FT-STS or ARPES) become negligible near the singularities of the CEC that is considered. This was *a priori* not obvious. Finally, going back to the first works of Friedel, our phenomenological interpretation of a JDOS picture based on a geometric construction is another experimental illustration of the generalization of Friedel oscillation to Bloch wave states, as described theoretically [18, 19] and encountered experimentally by the precursors of the FT-STS technique for complex Fermi surfaces [14]. Here we have demonstrated that not only the evolution of the power spectrum features but also their shape conceal information; furthermore, the robustness of the bands through the JDOS approach in a wide range of energy (-1, $+0.3$ eV) is demonstrated.

Acknowledgments

This work is supported by the Région Alsace and CNRS. We thank G Gewinner for very useful discussions and J C Peruchetti and S Zabrocki for their contribution to this work. We thank E Denys for technical support.

References

[1] Friedel J 1958 *Nuovo Cimento* **7** 287
[2] Ashcroft N W and Mermin M D 1987 *Solid State Physics* (Austin, TX: Holt, Rinehart and Winston) chapter 17
[3] Ruderman M A and Kittel C 1954 *Phys. Rev.* **96** 99
[4] Yosida K 1957 *Phys. Rev.* **106** 893

[5] Kasuya T 1956 *Prog. Theor. Phys.* **16** 45
[6] Knorr N, Brune H, Epple M, Hirstein A, Schneider M A and Kern K 2002 *Phys. Rev.* B **65** 115420
[7] Gautier F and Lenglart P 1965 *Phys. Rev.* A **139** 705
[8] Hasegawa Y and Avouris Ph 1993 *Phys. Rev. Lett.* **71** 1071
[9] Crommie M F, Lutz C P and Eigler D M 1993 *Nature* **363** 524
[10] Jeandupeux O, Bürgi L, Hirstein A, Brune H and Kern K 1999 *Phys. Rev.* B **59** 15926
[11] Bürgi L, Brune H and Kern K 2002 *Phys. Rev. Lett.* **89** 176801
[12] Sprunger P T, Petersen L, Plummer E W, Lægsgaard E and Besenbacher F 1997 *Science* **275** 1764
[13] Petersen L, Hofmann Ph, Plummer E W and Besenbacher F 2000 *J. Electron. Spectrosc. Relat. Mater.* **109** 97
[14] Hoffmann Ph, Brinner B G, Doering M, Rust H-P, Plummer E W and Bradshaw A M 1997 *Phys. Rev. Lett.* **79** 265
[15] Hoffman J E, McElroy K, Lee D-H, Lang K M, Eisaki H, Uchida S and Davis J C 2002 *Science* **297** 1148
[16] McElroy K, Simmonds R W, Hoffman J E, Lee D-H, Orenstein J, Elsaki H, Uchida S and Davis J C 2003 *Nature* **422** 592
[17] Pascual J I, Bihlmayer G, Koroteev Y M, Rust H P, Ceballos G, Hansmann M, Horn K, Chulkov E V, Blügel S, Echenique P M and Hofmann Ph 2004 *Phys. Rev. Lett.* **93** 196802
[18] Roth L M, Zeiger H J and Kaplan T A 1966 *Phys. Rev.* **16** 149
[19] Blandin A 1961 *Thesis* Universite de Paris sud Orsay, unpublished
[20] Stauffer L, Mharchi A, Pirri C, Wetzel P, Bolmont D, Gewinner G and Minot C 1993 *Phys. Rev.* B **47** 10555
[21] Wetzel P, Pirri C, Paki P, Peruchetti J C, Bolmont D and Gewinner G 1992 *Solid State Commun.* **82** 235
[22] Wetzel P, Pirri C, Gewinner G, Pelletier S, Roge P, Palmino F and Labrune J C 1997 *Phys. Rev.* B **56** 9819
[23] Tuilier M-H, Wetzel P, Pirri C, Bolmont D and Gewinner G 1994 *Phys. Rev.* B **50** 2333
[24] Lohmeier M, Huisman W J, terHorst G, Zagwijn P M, Vlieg E, Nicklin C L and Turner T S 1996 *Phys. Rev.* B **54** 2004
[25] Spence D J, Tear S P, Noakes T C Q and Bailey P 2000 *Phys. Rev.* B **61** 5707
[26] Vonau F, Aubel D, Gewinner G, Pirri C, Peruchetti J C, Bolmont D and Simon L 2004 *Phys. Rev.* B **69** 081305R
[27] Vonau F, Aubel D, Gewinner G, Peruchetti J C, Bolmont D and Simon L 2005 *Phys. Rev. Lett.* **95** 176803
[28] Brihuega I, mallet P, Magaud L, Pons S, Custance O, Gomez-Rodriguez J M and Veuillen J-Y 2004 *Phys. Rev.* B **69** 155407
[29] Wang Q-H and Lee D-H 2003 *Phys. Rev.* B **67** 02511R
[30] Markiewicz R S 2004 *Phys. Rev.* B **69** 214517
[31] McElroy K, Gweon G-H, Zhou S Y, Graf J, Uchida S, Eisaki H, Takagi H, Sasagawa T, Lee D-H and Lanzara A 2006 *Phys. Rev. Lett.* **96** 067005
[32] Li J *et al* 1997 *Phys. Rev.* B **56** 7656
[33] Rogero C, Koitzsch C, Gonzalez M E, Aebi P, Cerda J and Martin-Gago J A 2004 *Phys. Rev.* B **69** 045312
[34] Capriotti L, Scalapino D J and Sedgewick R D 2003 *Phys. Rev.* B **68** 014508
[35] Kodra O and Atkinson W A 2006 *Phys. Rev.* B **73** 045404
[36] http://www.lpse.uha.fr/Groupe%20LT%20STM-STS/Home.htm